HYDROGEN FUEL CELL & ENERGY STORAGE

Performance assessment of a power/refrigeration cogeneration system driven by the waste heat of a solid oxide fuel cell

Armin Emamifar

Mechanical Engineering Department, Ayatollah Boroujerdi University, Boroujerd, Iran.emamifar@abru.ac.ir

Article Information

Article Type:
Research Article

Article History:

Received: 25 June 2023
Received in revised form
17 Augest 2023
Accepted: 17 September 2023
Published on line 28 September 2023

Keywords

Solid oxide fuel cell
ORC
VCR
exergy analysis

Abstract

A combination of a solid oxide fuel cell with two CCP subsystems to generate power and refrigeration is investigated in the present paper. The proposed system consists of two combined ORC-VCR systems whose input energy is supplied by the waste heat of a SOFC. Energy and exergy analysis was carried out for the system components. The results indicate that by recovering the waste heat of the SOFC, the energy and exergy efficiencies are improved by 45.82% and 6.14% compared to the stand-alone SOFC system. In addition, the proposed system can generate 382.4kW power and 176.28kW refrigeration, respectively. Moreover, the exergy analysis demonstrates that the air heat exchanger, afterburner, SOFC stack, and evaporatorI have a considerable exergy destruction rate compared to other system components. The effects of key parameters of the SOFC and ORC-VCR subsystems on the system performance are also analyzed. The results revealed that increasing current density increases SOFC net power and refrigeration capacity. Furthermore, by increasing the SOFC operating temperature, the refrigeration capacity increases. However, an optimum value for the cell operating temperature produces the maximum SOFC net power.

Cite this article: Emamifar, A. (2023). Performance assessment of a power/refrigeration cogeneration system driven by the waste heat of a solid oxide fuel cell. DOI:10.22104/HFE.2023.6184.1260

Publisher:Iranian Research Organization for Science and Technology(IROST)
DOI:10.22104/HFE.2023.6184.1260

1. Introduction

The reduction in fossil fuels, environmental issues, global warming, and the need for more efficient systems have resulted in consideration of new energy sources over the past few decades [1, 2]. Among many renewable energies, solid oxide fuel cells have several benefits like high efficiency, high operating temperature, low noise and pollution, and high power density [3-8]. Besides, due to the high exhaust temperature in this component, its waste gases have enough energy to be further recovered by other systems to produce power, refrigeration, hydrogen, fresh water, etc. [9-22]. Wang et al. [23] introduced a hybrid system in which the waste energy of a SOFC-GT was delivered to a Kalina cycle. They investigated the effect of different parameters like compressor pressure ratio and air flow rate on the system's performance. Yan et al. [24] integrated a SOFC, a gas turbine, and an ORC with LNG as a heat sink to generate more power. The net system electrical efficiency was reported at 67%. Zhao et al. [25] studied a CCHP combined with a SOFC to obtain more efficiency. They indicated that the electrical efficiency of the SOFC, the total power efficiency, and the overall efficiency of the SOFC-CCHP are 60%, 70%, and 90%, respectively. Chitsaz et al. [26] introduced four different hybrid systems based on a SOFC. Energy, exergy, and economic analysis were performed, and the results were compared for different configurations. They demonstrated that the cathode and anode gas recycling system produced better results. Chitgar et al. [27] employed a Kalina cycle, a SOFC, and a thermoelectric generator in a hybrid system. The power generated by the Kalina and thermoelectric generator was transmitted to a reverse osmosis desalination system. The total cost rate and energy efficiency were reported as 36.8 $/hr and 54%, respectively.

Emadi et al. [28] proposed a hybrid system based on a dual loop ORC and SOFC-GT. An LNG system was also used as the ORC's heat source, and some electricity was produced through the LNG turbine. The system performance was evaluated for different working fluids in the ORC. Adebayo et al. [29] proposed a mutigeneration system consisting of a cascaded closed loop ORC, a SOFC, a LiBr/water absorption refrigeration system, a biogas digester, and a PEM electrolyzer; the SOFC was the main mover. They investigated the thermodynamic performance of the system for different design parameters. Zeng et al. [30] presented a hybrid system based on a SOFC, a gas turbine, an ORC, and a double-effect absorption refrigeration system. They obtained 48.2%, 63.2%, and 62.67% for SOFC electrical efficiency and the system's overall electrical and exergy efficiency, respectively. Zhong et al. [31] proposed a hybrid system based on a SOFC, supercritical CO2 system, and an ejector refrigeration system. The results showed that the SOFC has the highest cost and exergy destruction rate compared to the other subsystems. Dhahad et al. [32] proposed a novel CCP system based on a SOFC, an ejector, and an absorption refrigeration system. They stated that increasing the evaporation temperature, the ammonia concentration, and the SOFC inlet temperature can result in higher exergy productivity. Mei et al. [33] employed a thermoelectric generator and an absorption refrigeration system to use the waste energy of a SOFC system. They introduced

four different configurations for the system and compared their thermodynamic performances. Song et al. [34] employed a Rankin and Kalina cycle as the top and bottom systems to achieve the waste energy of a SOFC. The genetic algorithm was employed to optimize the thermodynamic parameters. The generated power of the SOFC, Kalina cycle, and Rankin cycle was 145 kW, 59.39 kW, and 170.1 kW, respectively.

As mentioned above, many studies have been done on integrating a SOFC with other thermodynamic systems, and the design of multipurpose systems has always been of great importance. The present research investigates a novel integrated system that integrates a SOFC system with two ORC-VCR subsystems. The proposed cogeneration system has the ability to produce power or combined power and refrigeration in a wide range of refrigeration temperatures. Thermodynamic modeling is conducted to obtain energy and exergy efficiencies of the system. Additionally, a parametric analysis is carried out to investigate the effect of important parameter variations on system performance.

2. System description

Fig. 1 illustrates the CCP system considered in the present work. The SOFC unit produces power and the two ORC-VCR subsystems supply refrigeration employing the energy of waste gases from the SOFC. Air and fuel (methane) enter the air compressor (AC) and fuel compressor (FC), respectively, and reach the required pressure of the SOFC. The air enters the cathode of the SOFC after preheating in the HEX3. The fuel also preheats in the HEX2 and then mixes with water, which is pumped and passed through the HEX1. The mixed stream enters the anode of the SOFC. Due to electrochemical reactions occurring in the SOFC unit, DC current is produced. Then, an inverter will convert it to AC current. After finishing the electrochemical reactions in the SOFC, the unreacted fuel and excess air reach the afterburner, where the high-temperature combustion gases and pressure preheat the water, the fuel, and the air, respectively. Since the flue gases retain a high temperature after passing through the HEX3, they can enter the vapor generator I of a combined ORC-VCR system with a regenerator to produce refrigeration. The organic fluid superheated in vapor generator I enters turbine I to generate power and mixes with the compressor I outlet after passing through the regenerator (HEX4) before flowing to the condenser. The saturated liquid exiting the condenser splits into two streams. One stream goes to the vapor generator I, and the other passes through expansion valve I and enters evaporator I. The saturated vapor outlet of the evaporator enters the compressor and is pressurized to the condenser pressure. The flue gases exiting vapor generator I then flows to vapor generator II to run the second ORC-VCR system in which the regenerator is removed due to operating temperature.

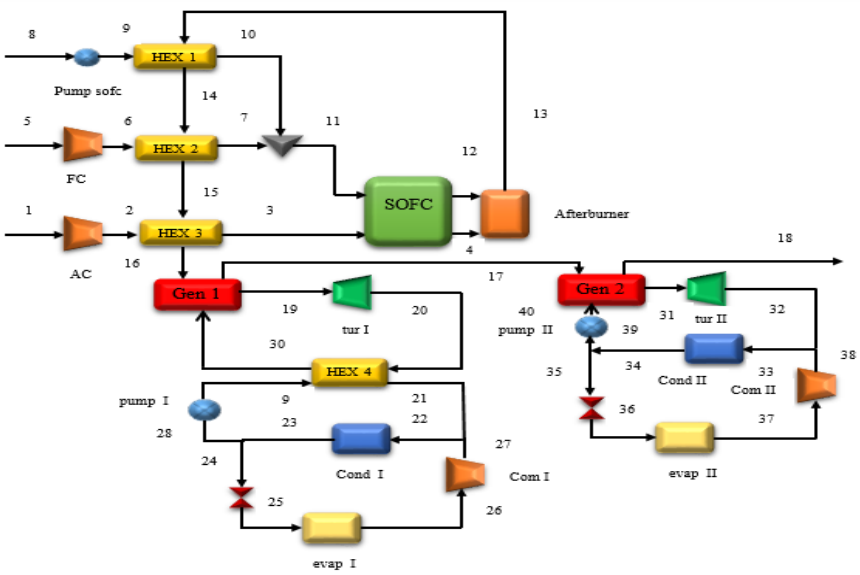

Fig. 1. The schematic of the SOFC integrated with two ORC-VCR systems.

3. Thermodynamic modeling

Some of the thermodynamic simulation assumptions are listed as follows [23, 26, 27, 29, 32] :

- The system reaches a steady condition.
- The air consists of 79% N_2 and 21% O_2.
- Fuel and air entering the SOFC have equal temperature and pressure.
- The constant resistance and the pressure change throughout the SOFC are neglected.
- The unreacted gases are completely oxidized in the afterburner.
- The pressure losses in the pipelines and heat exchangers are neglected.

The reactions that occurred in the SOFC are as follows:

$$\begin{aligned} x_r &\rightarrow [CH_4 + H_2O \rightarrow CO + 3H_2] \\ y_r &\rightarrow [CO + H_2O \rightarrow H_2 + CO_2] \\ z_r &\rightarrow \left[H_2 + \frac{1}{2}O_2 \rightarrow H_2O\right] \end{aligned} \quad (1)$$

Where xr, yr, and zr denote the level of the reforming reaction, shifting reaction, and overall reaction, respectively. Equation (2) indicates the required equations for mass balance in the main components of the system:

$$\begin{aligned} \dot{n}_{CH_4,in} &= x_r \\ \dot{n}_{H_2O,in} &= 2.5x_r \\ \dot{n}_{H_2,out} &= 3x_r - y_r - z_r \\ \dot{n}_{CO,out} &= x_r - y_r \\ \dot{n}_{CO_2,out} &= y_r \\ \dot{n}_{H_2O,out} &= 2.5x_r - y_r - z_r \\ z_r &= U_f\left(3x_r + y_r\right) \end{aligned} \quad (2)$$

Where n is the molar flow rate and U_f depicts the fuel consumption factor. The following equation shows the SOFC stack work:

$$\dot{W}_{FC,stack} = N_{cell}.I.V_{cell} \quad (3)$$

Where V_{cell} represents the voltage of the fuel cell and can be derived as:

$$V_{cell} = V_N - V_{loss} \tag{4}$$

Where V_N is reversible voltage and V_{loss} depicts the voltage losses. The relations required to compute the voltage of the fuel cell are presented in Table 1.

Table 1. Calculation of V_{cell}.

Voltage	Relation
Nernst voltage	$E_{Nernst} = \frac{-\Delta G^0}{n_e F} + \frac{RT_{fc}}{n_e F}\ln\left(\frac{P_{H_2}\left(P_{O_2}\right)^{0.5}}{P_{H_2O}^{sat}}\right)$
Ohmic voltage	$V_{loss} = V_{act} + V_{ohm} + V_{conc}$ $V_{ohm} = \left(\rho_a l_a + \rho_c l_c + \rho_e l_e + \rho_{\text{int}} l_{\text{int}}\right) i$ $\rho_a = \left(\frac{95\times10^6}{T_{cell}}\exp\left(\frac{-1150}{T_{cell}}\right)\right)^{-1}$ $\rho_c = \left(\frac{42\times10^6}{T_{cell}}\exp\left(\frac{-1200}{T_{cell}}\right)\right)^{-1}$ $\rho_e = \left(3.34\times10^4\exp\left(\frac{-10300}{T_{cell}}\right)\right)^{-1}$ $\rho_{\text{int}} = \left(\frac{9.3\times10^6}{T_{cell}}\exp\left(\frac{-1100}{T_{cell}}\right)\right)^{-1}$
Activation voltage	$V_{act} = V_{act,a} + V_{act,c}$ $V_{act,a} = \frac{RT_{cell}}{F}\left(\sinh^{-1}\left(\frac{i}{2i_{oa}}\right)\right)$ $V_{act,c} = \frac{RT_{cell}}{F}\left(\sinh^{-1}\left(\frac{i}{2i_{oc}}\right)\right)$
Concentration voltage	$V_{conc} = V_{conc,a} + V_{conc,c}$ $V_{conc,a} = \frac{-RT_{cell}}{2F}\left(\ln\left(1-\frac{i}{i_{as}}\right) - \ln\left(1-\frac{P_{H_2} i}{P_{H_2O} i_{as}}\right)\right)$ $V_{conc,c} = \frac{-RT_{cell}}{4F}\left(\ln\left(1-\frac{i}{i_{cs}}\right)\right)$ $i_{as} = \frac{4FP_{H_2} D_{aeff}}{RT_{cell} l_a}$ $i_{cs} = \frac{4FP_{O_2} D_{ceff}}{RT_{cell} l_c\left(1-\frac{P_{O_2}}{P_0}\right)}$

The current and current density of the SOFC stack can be written as:

$$I = i.A_a$$
$$i = \frac{2.F.z_r}{N_{cell}.A_a} \tag{5}$$

Where F, N_{fc}, and A_a are the Faraday, constant, and number of cells, respectively. The energetic analysis is based on the first law of thermodynamics and can determine the heat transfer and work rate occurring in each system component. Moreover, the exergy analysis, based on the second law of thermodynamics, is essential to identify losses, wastes, and irreversibilities arising in the system. In order to analyze the system's energy and exergy performance, the mass balance and the energy and exergy equations are applied to each system component.

$$\sum \dot{m}_i - \sum \dot{m}_e = 0 \tag{6}$$

$$\sum \dot{m}_i h_i - \sum \dot{m}_e h_e + \sum \dot{Q} - \sum \dot{W} = 0 \tag{7}$$

$$\dot{E}_d = \dot{E}_{in} - \dot{E}_{out} + \dot{E}_Q + \dot{E}_W \tag{8}$$

The exergy of each point of the system can be obtained as follows:

$$ex = ex_{ph} + ex_{ch} \tag{9}$$

Where ex_{ph} and ex_{ch} depicts physical and chemical exergy, respectively, which can be expressed using the following equations:

$$ex_{ph} = \left(h - h_0\right) - T_0\left(s - s_0\right) \tag{10}$$

$$ex_{ch} = \sum x_n ex_{ch,n} + RT_0 \sum x_n \ln x_n \tag{11}$$

Where x_n is the mole fraction of species n, and $ex_{ch,n}$ is the chemical exergy of species n in a dead state. The standard chemical exergies can be found in [35]. The equations for energy and exergy of each part of the system are presented in Table 2.

Table 2. Exergy and exergy equations for the system components.

Component	Energy equation	Exergy equation
HEX I	$\dot{Q}_{HEX1} = \dot{m}_{13}\left(h_{13} - h_{14}\right)$	$\dot{E}x_9 - \dot{E}x_{10} + \dot{E}x_{13} - \dot{E}x_{14} = \dot{E}_{D,HEX1}$
HEX 2	$\dot{Q}_{HEX2} = \dot{m}_{13}\left(h_{14} - h_{15}\right)$	$\dot{E}x_6 - \dot{E}x_4 + \dot{E}x_{14} - \dot{E}x_{15} = \dot{E}_{D,HEX2}$
HEX 3	$\dot{Q}_{HEX3} = \dot{m}_{13}\left(h_{15} - h_{16}\right)$	$\dot{E}x_2 - \dot{E}x_3 + \dot{E}x_{15} - \dot{E}x_{16} = \dot{E}_{D,HEX3}$
AC	$\dot{W}_{AC} = \dot{m}_1\left(h_2 - h_1\right)$ $\eta_{AC} = \dfrac{h_{2s} - h_1}{h_2 - h_1}$	$\dot{E}x_1 + \dot{W}_{AC} = \dot{E}x_2 + \dot{E}_{D,AC}$
FC	$\dot{W}_{FC} = \dot{m}_5\left(h_6 - h_5\right)$ $\eta_{FC} = \dfrac{h_{6s} - h_5}{h_6 - h_5}$	$\dot{E}x_5 + \dot{W}_{FC} = \dot{E}x_6 + \dot{E}_{D,FC}$
Pump sofc	$\dot{W}_{pump,sofc} = \dot{m}_8\left(P_9 - P_8\right)/\rho\eta_p$ $\dot{W}_{Pump,sofc} = \dot{m}_8\left(h_9 - h_8\right)$	$\dot{E}x_8 = \dot{E}x_9 - \dot{W}_{Pump,sofc} + \dot{E}_{D,pump,sofc}$
Mixer	$\dot{m}_{11}h_{11} = \dot{m}_7h_7 + \dot{m}_{10}h_{10}$	$\dot{E}x_7 + \dot{E}x_{10} = \dot{E}x_{11} + \dot{E}_{D,Mixer}$
SOFC	$\dot{Q}_{evp} = \dot{m}_7\left(h_8 - h_7\right)$	$\dot{E}x_3 - \dot{E}x_4 + \dot{E}x_{11} - \dot{E}x_{12} = \dot{E}_{D,SOFC}$
Afterburner	$h_6 = h_7$	$\dot{E}x_4 + \dot{E}x_{12} = \dot{E}x_{13} + \dot{E}_{D,Afterburner}$
Generator I	$\dot{Q}_{genI} = \dot{m}_{16}\left(h_{16} - h_{17}\right) = \dot{m}_{30}\left(h_{19} - h_{30}\right)$	$\dot{E}x_{16} - \dot{E}x_{17} + \dot{E}x_{30} - \dot{E}x_{19} = \dot{E}_{D,GeneratorI}$
Turbine I	$\dot{W}_{turI} = \dot{m}_{19}\left(h_{19} - h_{20}\right)$	$\dot{E}x_{19} = \dot{E}x_{20} + \dot{W}_{turI} + \dot{E}_{D,turI}$
Evaporator I	$\dot{Q}_{evapI} = \dot{m}_{25}\left(h_{26} - h_{25}\right)$	$\dot{E}x_{25} + \dot{Q}_{evpI}\left(1 - \dfrac{T_0}{T_{evpI}}\right) = \dot{E}x_{26} + \dot{E}_{D,evpI}$
Condenser I	$\dot{Q}_{condI} = \dot{m}_{22}\left(h_{22} - h_{23}\right)$	$\dot{E}x_{22} + \dot{Q}_{condI}\left(1 - \dfrac{T_0}{T_{condI}}\right) = \dot{E}x_{23} + \dot{E}_{D,CondI}$
Expansion valve I	$h_{24} = h_{25}$	$\dot{E}x_{24} = \dot{E}x_{25} + \dot{E}_{D,ValveI}$
HEX 4	$h_{20} - h_{21} = h_{30} - h_9$	$\dot{E}x_{20} - \dot{E}x_{21} + \dot{E}x_9 - \dot{E}x_{30} = \dot{E}_{D,HEX4}$
Generator II	$\dot{Q}_{genII} = \dot{m}_{16}\left(h_{17} - h_{18}\right) = \dot{m}_{40}\left(h_{31} - h_{40}\right)$	$\dot{E}x_{17} - \dot{E}x_{18} + \dot{E}x_{40} - \dot{E}x_{31} = \dot{E}_{D,GeneratorII}$
Turbine II	$\dot{W}_{turII} = \dot{m}_{31}\left(h_{31} - h_{32}\right)$	$\dot{E}x_{31} = \dot{E}x_{32} + \dot{W}_{turII} + \dot{E}_{D,turII}$
Evaporator II	$\dot{Q}_{evapII} = \dot{m}_{36}\left(h_{37} - h_{36}\right)$	$\dot{E}x_{36} + \dot{Q}_{evpII}\left(1 - \dfrac{T_0}{T_{evpII}}\right) = \dot{E}x_{37} + \dot{E}_{D,evpII}$
Condenser II	$\dot{Q}_{condII} = \dot{m}_{33}\left(h_{33} - h_{34}\right)$	$\dot{E}x_{33} + \dot{Q}_{condII}\left(1 - \dfrac{T_0}{T_{condII}}\right) = \dot{E}x_{34} + \dot{E}_{D,CondII}$
Expansion valve II	$h_{35} = h_{36}$	$\dot{E}x_{35} = \dot{E}x_{36} + \dot{E}_{D,ValveII}$

The efficiency of the ORC-EVCR and the total efficiency of the system can be calculated through the following equations:

$$COP = \frac{\dot{Q}_{evp}}{\dot{Q}_{gen} + \dot{W}_{pump}} \quad (12$$

$$\eta_{SOFC} = \frac{\dot{W}_{SOFC} - \dot{W}_{AC} - \dot{W}_{FC} - \dot{W}_{pump,sofc}}{\left(\dot{m}_{H_2,cons}\right).LHV_{CH_4}} \quad (13$$

$$\eta_{Overall} = \frac{\dot{W}_{SOFC} - \dot{W}_{AC} - \dot{W}_{FC} - \dot{W}_{pump,sofc} + \dot{Q}_{evpI} + \dot{Q}_{evpII} - \dot{W}_{pumpI} - \dot{W}_{pumpII}}{\left(\dot{m}_{H_2,cons}\right).LHV_{CH_4}} \quad (14$$

Moreover, the exergy efficiency of the ORC-EVCR, PEM fuel cell, and total system can be calculated as follows:

$$\eta_{x,SOFC} = \frac{\dot{W}_{SOFC} - \dot{W}_{AC} - \dot{W}_{FC} - \dot{W}_{pump,sofc}}{(\dot{E}x_3 + \dot{E}x_{11}) - (\dot{E}x_4 + \dot{E}x_{12})} \quad (15$$

$$\eta_{x,ORC-EVCRI} = \frac{\dot{Q}_{evpI}\left(1 - \frac{T_0}{T_{evpI}}\right)}{(\dot{E}x_{16} + \dot{E}x_{17}) - (\dot{E}x_{30} + \dot{E}x_{19}) + \dot{W}_{pumpI}} \quad (16$$

$$\eta_{x,ORC-EVCRII} = \frac{\dot{Q}_{evpII}\left(1 - \frac{T_0}{T_{evpII}}\right)}{(\dot{E}x_{17} + \dot{E}x_{18}) - (\dot{E}x_{40} + \dot{E}x_{31}) + \dot{W}_{pumpII}} \quad (17$$

$$\eta_{x,overall} = \frac{\dot{W}_{SOFC} - \dot{W}_{AC} - \dot{W}_{FC} - \dot{W}_{pump,sofc} + \dot{Q}_{evpI}\left(1 - \frac{T_0}{T_{evpI}}\right) + \dot{Q}_{evpII}\left(1 - \frac{T_0}{T_{evpII}}\right) - \dot{W}_{pumpI} - \dot{W}_{pumpII}}{(\dot{E}x_3 + \dot{E}x_{11}) - (\dot{E}x_4 + \dot{E}x_{12})} \quad (18$$

4. Results and discussion

This section presents and discusses the thermodynamic modeling results and the effect of variations in important parameters on system performance. The EES program was employed to perform all thermodynamic computations. In order to validate the mathematical model of the proposed system, the SOFC voltage is compared with data presented by Ref [29]. According to Fig. 2, there is an acceptable agreement between the results of the current study and those reported by [29]. Moreover, the ORC-VCR simulation was verified by comparing the main thermodynamic parameters with the results from [36] for the R245fa refrigerant. As can be seen in Table 3, the maximum deviation is 0.35%, which indicates good consistency between the results. The required input parameters for simulation are listed in Table 4. Considering the temperature range, cyclohexane and propane were selected as the working fluid in the ORC-VCR 1 and ORC-VCR2 subsystems, respectively. Table 5 shows that the SOFC system can generate 382.4 kW power. In addition, 159.9 kW and 16.38 kW of refrigeration load can be produced by integrating two ORC-VCRI and ORC-VCRII subsystems, respectively. Moreover, the proposed system's overall energy and exergy efficiencies are 68.96% and 81.89%, respectively, 45.82% and 6.14% higher than the stand-alone SOFC system. Fig. 3 represents the distribution of exergy destruction rate for each system component. It can be observed that the largest amount of exergy destruction occurs in the HEX3, which is about 20.41% of the total exergy destruction rate. Furthermore, the afterburner, SOFC stack, and evaporator I also have considerable destroyed exergy, which should be considered in the design and application of the system.

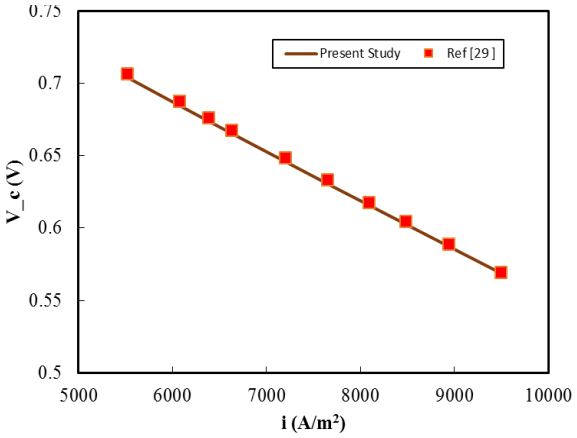

Fig. 2. SOFC voltage verification by [29].

Table 3. Comparison of ORC-VCR cycle parameters with Ref [36]

Parameter	Present study	Ref [36]	Deviation (%)
$\dot{W}_{turbine}$ (kW)	31.35	31.39	0.12
$\dot{Q}_{evp}$ (kW)	158.57	158.7	0.08
COP_s	0.5815	0.582	0.08
η_x (%)	30.57	30.68	0.36

Table 4. The input parameters for the simulation [26, 29, 32].

Parameter	Value
Farady Constant, F	96485 (C/mol)
Number of electrons, n_e	2
Number of cells, N_{cell}	13000
Difference temperature between inlet and outlet of SOFC	100 (°C)
Active surface area, A_a	0.01 (m^2)
Current density	5500 (A/ m^2)
Anode exchange current density, i_{oa}	6500 (A/ m^2)
Cathode exchange current density, i_{oc}	2500 (A/ m^2)
η_{inv}	95 %
Effective anode gaseous diffusivity, D_{aeff}	0.2×10^{-4} (m^2/s)
Effective cathode gaseous diffusivity, D_{ceff}	0.05×10^{-4} (m^2/s)
Fuel utilization factor, U_f	0.8
Anode thickness, l_a	0.05 (cm)
Cathode thickness, l_c	0.005 (cm)
Electrolyte thickness, l_e	0.001 (cm)
Interconnect thickness, l_{int}	0.3 (cm)
Steam to carbon ratio, r_{sc}	2
Afterburner efficiency, η_{AB}	99 %
η_{AC}	85 %
η_{FC}	85 %
η_p	85 %
Inlet pressure of turbine I	622 kPa
Inlet pressure of turbine II	2667 kPa
Degree of superheat	10 (°C)
Pinch point temperature in generators	10 (°C)

Table 5. Result of energy and exergy analysis for the proposed system.

Parameter	Value
SOFC voltage (V)	0.7049
SOFC net electrical power (kW)	382.4
SOFC energy efficiency (%)	47.29
SOFC exergy efficiency (%)	77.15
SOFC exergy destruction rate (kW)	354.87
ORC-VCRI COP	0.79
$\dot{Q}_{evpI}$ (kW)	159.9
ORC-VCRI exergy efficiency	24.09
ORC-VCRI exergy destruction rate (kW)	131.5
ORC-VCRII COP	0.27
$\dot{Q}_{evpII}$ (kW)	16.38
ORC-VCRII exergy efficiency (%)	15.64
ORC-VCRII exergy destruction rate (kW)	29.04
Overall energy efficiency (%)	68.96
Overall exergy efficiency (%)	81.89
Overal exergy destruction rate (kW)	515.41

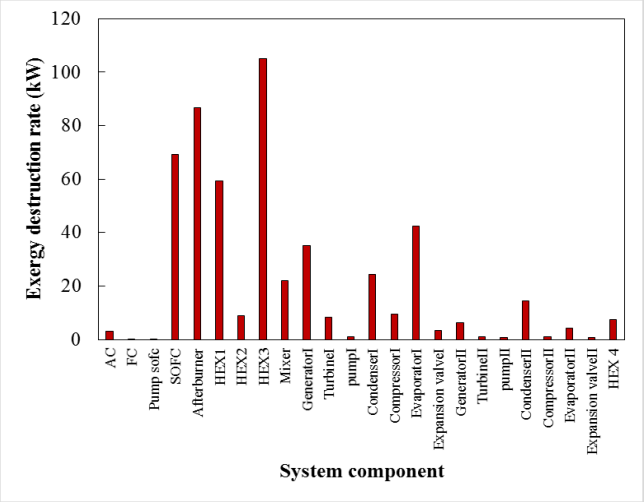

Fig. 3. Exergy destruction rates of the system components.

5. Parametric Study

Fig. 4 shows the variations of SOFC net power generation and the refrigeration capacity of the system while the other operating parameters are kept constant. As observed, the net power generation of the SOFC and refrigeration capacity increases with increasing the current density. Increasing the fuel cell current density increases the voltage losses, leading to a reduction in the fuel cell voltage. However, the effect of increasing the current density is more prominent than decreasing the fuel cell voltage. Therefore, the net power of the

SOFC increases with increasing the current density. Furthermore, increasing the current density increases the molar flow rate to the SOFC, which increases heat energy delivered to the two ORC-VCR subsystems, raising the refrigeration capacity. However, as can be observed from Fig. 4b, the energy and exergy efficiency of the system decrease with increasing the current density. This is because increasing the rate of inlet energy and exergy is greater than outlet energy and exergy from the fuel cell. Hence, the efficiency of the SOFC and the total system efficiency decrease.

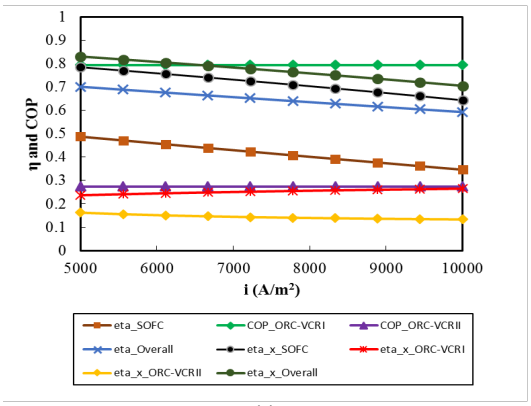

(a)

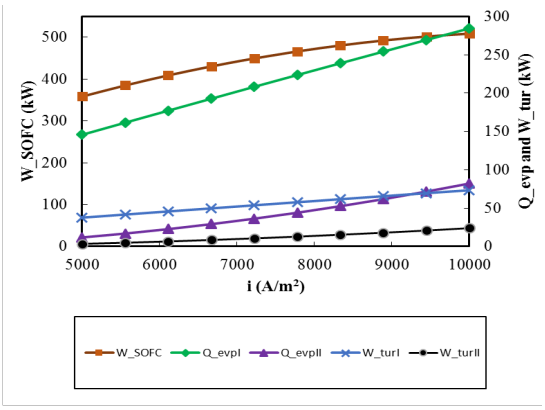

(b)

Fig. 4. Effect of current density variation on a) system performance and b) power and refrigeration capacity.

The variations in the system performance with fuel cell inlet temperature are displayed in Fig. 5. As can be observed from Fig. 5a, increasing the fuel cell inlet temperature first increases then decreases the fuel cell output power. This is because increasing the fuel cell inlet temperature causes a decrease in the Ohm voltage and increases the activation and concentration voltages. Hence, there is an optimum value for the fuel cell voltage and fuel cell power. Referring to Fig. 5b, Q_{evpI} increases and Q_{evpII} decreases with increasing the fuel cell inlet temperature. At higher fuel cell inlet temperatures, the temperature of the fuel cell's exhaust gases increase, which leads to an increase in the inlet temperature of turbine I and, consequently, the refrigeration capacity of cycle I increases. On the other hand, increasing generator I's inlet temperature decreases the temperature of its outlet stream, which causes a decrease in the power of turbine II, decreasing the refrigeration capacity of cycle II.

Fig. 6 depicts the effect of the utilization factor on system performance. Referring to Fig. 6a, increasing

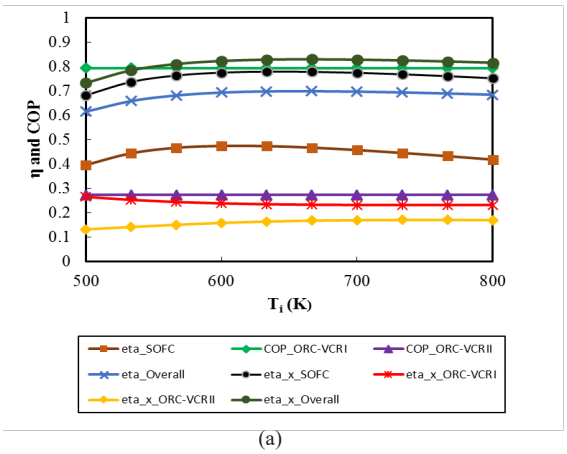

(a)

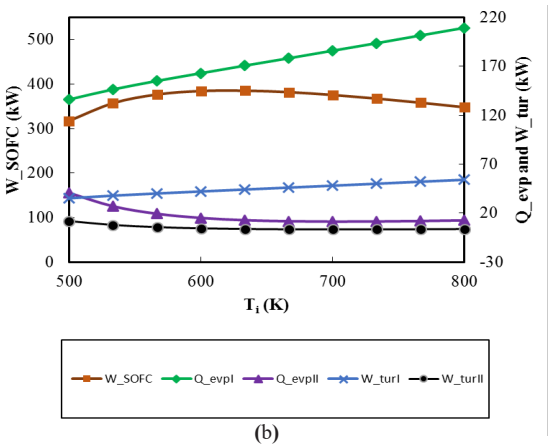

(b)

Fig. 5. Effect of fuel cell temperature variation on a) system performance and b) power and refrigeration capacity.

the fuel utilization factor decreases the SOFC net power and the refrigeration capacity. The reason is that in higher fuel utilization factors, the molar input rate of the fuel to the SOFC decreases, and the molar input rate of the air to the SOFC increases. Moreover, due to the participating hydrogen in the reactions, the partial pressure of the hydrogen and oxygen decreases, leading to a decrease in the SOFC voltage. Therefore, the output power of the SOFC decreases by increasing the fuel utilization factor. On the other hand, increasing the fuel utilization factor decreases the input energy to the ORC-VCR subcycles, which lowers the refrigeration capacity. However, the energy efficiency of the total system first increases and then declines as the utilization factor increases. This is because the reduction in the input fuel flow rate dominates the decreasing SOFC power. However, at higher utilization factors, the reduction of the input fuel flow rate cannot compensate for the reduced SOFC power, and the energy efficiency of the SOFC and hybrid system decline. Moreover, increasing the utilization factor decreases the exergy difference between the inlet and outlet streams of the SOFC. However, the reduction in power generation and refrigeration capacity is more prominent. Therefore, the exergy efficiency of the SOFC and the total system decrease as the utilization factor increases.

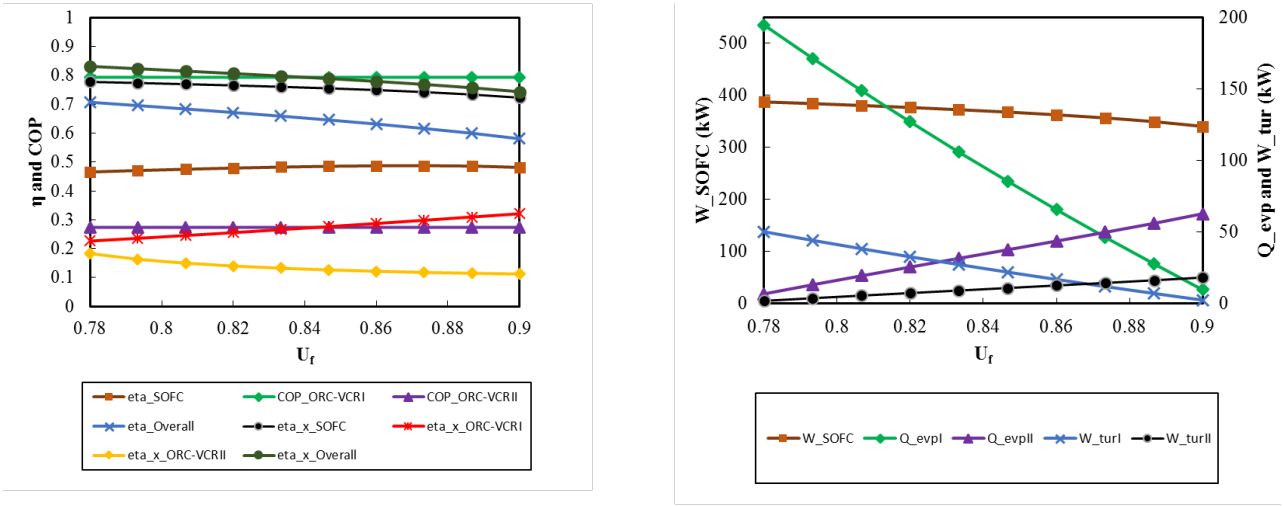

(a) (b)

Fig. 6. Effect of fuel utilization factor variation on a) system performance and b) power and refrigeration capacity.

The effect of the maximum pressure of the ORC-VCR I subcycle on system performance is displayed in Fig. 7. According to Fig. 6a, an increase in the inlet pressure of turbine I decreases the Q_{evpI} and increases the Q_{evpII}. Increasing the maximum pressure in ORC-VCR I at constant pinch temperature in generator I increases the output temperature of generator I, decreasing energy delivery to the ORC-VCR I and the refrigeration capacity. However, increasing the output temperature of the gases exiting generator I transfers more energy to the ORC-VCRII, and Q_{evpII} increases. Referring to Fig. 4b, there is an optimum value for the maximum pressure of the ORC-VCRI cycle at which the energy and exergy efficiencies of the system are maximum.

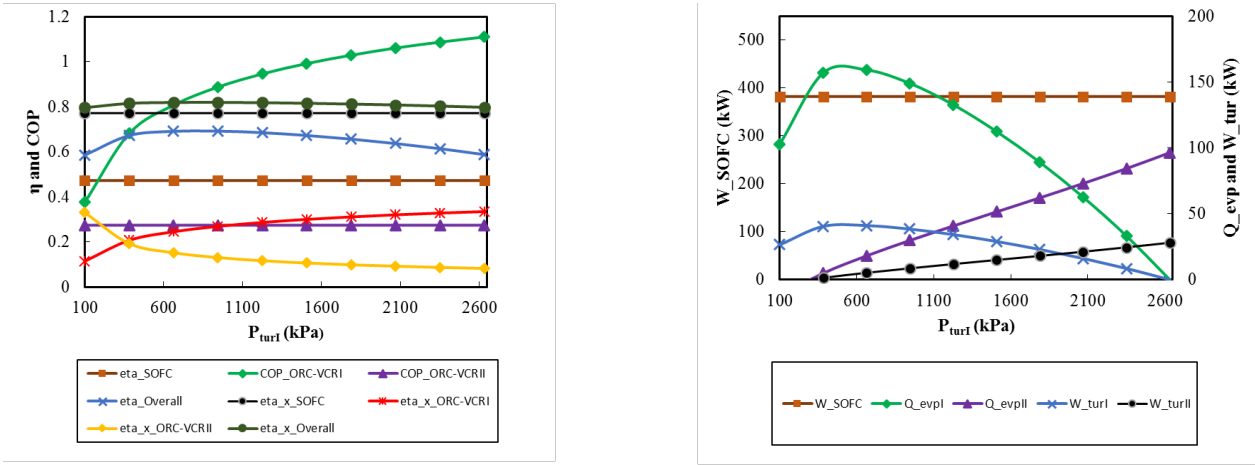

(a) (b)

Fig. 7. Effect of turbine I pressure variation on a) system performance and b) power and refrigeration capacity.

Fig. 8 depicts the effect of turbine II inlet pressure on system performance. As can be observed from Fig. 8a, the refrigeration capacity of ORC-VCRII increases as the maximum pressure increases. Whereas the SOFC and the ORC-VCRI parameters remain constant, the energy and exergy efficiencies of the system are enhanced at higher ORC-VCR II subsystem maximum pressures.

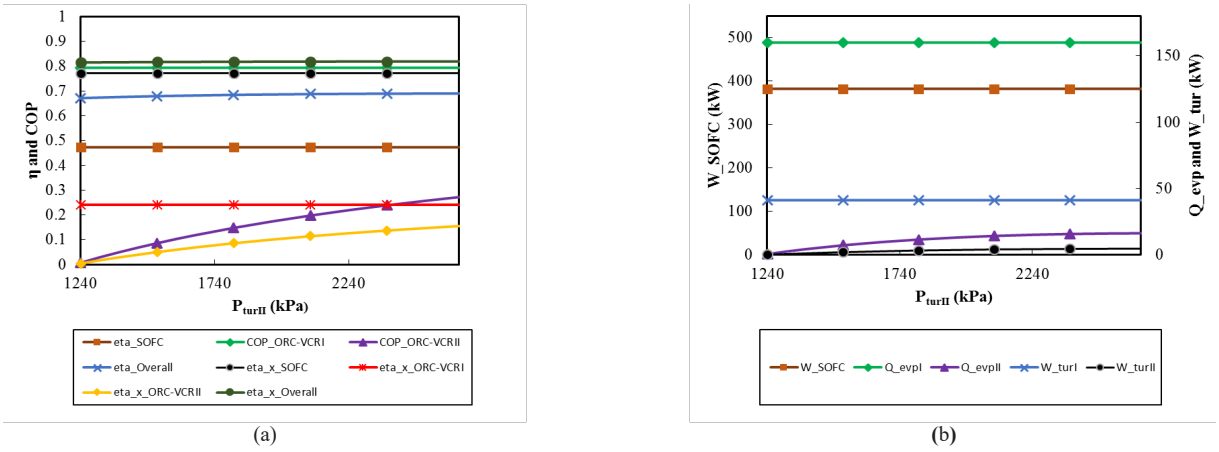

(a) (b)

Fig. 8. Effect of turbine II pressure variation on a) system performance and b) power and refrigeration capacity.

The impacts of evaporating temperature on system performance are displayed in Fig. 9. As can be seen, the energy and exergy efficiencies of the refrigeration capacity of both subsystems improve as the evaporator temperature rises. As the input energy to both ORV-VCR subsystems is constant, the variation of evaporator temperature has no influence on ORC sections. However, increasing the evaporator temperature increases the evaporator pressure, which leads to a reduction in required compressor power. Therefore, the mass flow rate of the refrigeration section increases. On the other hand, raising the evaporator pressure causes an increase in the enthalpy difference between the inlet and outlet streams of the evaporator. Increasing the mass flow rate and enthalpy difference along the evaporator improves the refrigeration capacity. As input parameters of the system are constant, energy and exergy efficiencies are enhanced as the evaporator temperature increases.

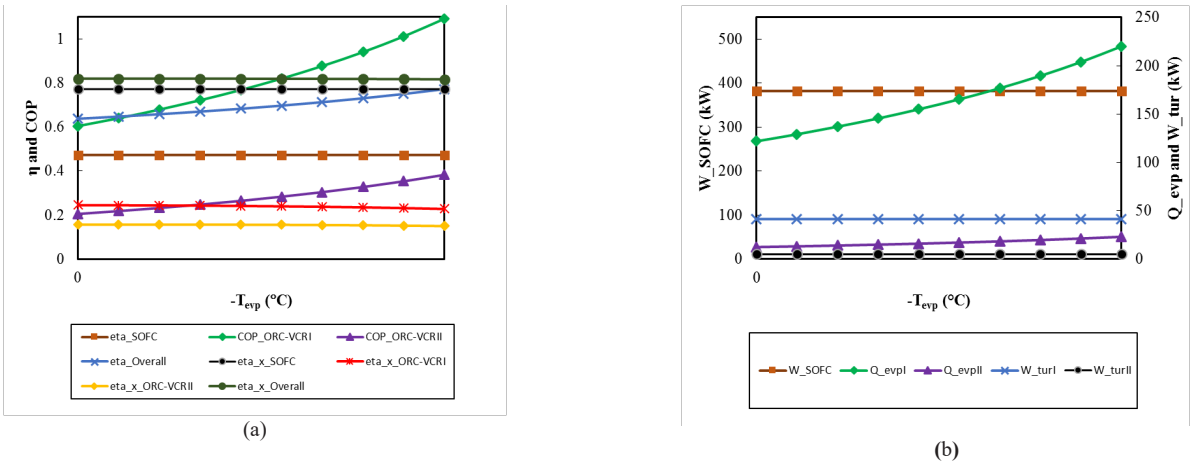

(a) (b)

Fig. 9. Effect of evaporator temperature variation on a) system performance and b) power and refrigeration capacity.

Conclusion

This work presents a CCP system consisting of a solid oxide fuel cell and two subsystems based on an organic Rankin cycle and vapor compression system. The SOFC produces electrical power, and the ORC-VCR subsystems use the waste heat of the solid oxide cell as a heat source to provide refrigeration. The energy and exergy efficiency of the proposed system was then compared to a stand-alone SOFC system. Afterward, a parametric study was carried out to investigate the effect of key thermodynamic parameters of the SOFC and ORC-VCR on system performance. The main conclusions of the present study can be summarized as follows:

- The system's overall energy and exergy efficiency is 45.82% and 6.14% higher than a stand-alone SOFC system.
- The refrigeration capacity and the energy and exergy efficiencies improve with rising the evaporator temperature.
- The net power generation of the SOFC and refrigeration capacity increases as the current density increases.
- There is an optimum cell operating temperature value to produce the maximum SOFC net power. This temperature for the mentioned input parameters is about 633 K.
- The SOFC net power and the refrigeration capacity decrease as the fuel utilization factor increases. Furthermore, the exergy efficiency of the SOFC and the total system decrease as the utilization factor increases.
- Overall, the system performance is enhanced at higher ORC-VCR II subsystem maximum pressures. However, there is an optimum maximum pressure value for the ORC-VCRI cycle at which the efficiencies of the system are maximum.

References

[1] Feng L., Dai X., Mo J, Shi L. "Analysis of energy-matching performance and suitable users of conventional CCHP systems coupled with different energy storage systems", Energy Conversion and Management, 2019, 200: 112093. https://doi.org/10.1016/j.enconman.2019.112093.

[2] Teke A, Timur O. "Assessing the energy efficiency improvement potentials of HVAC systems considering economic and environmental aspects at the hospitals", Renewable and Sustainable Energy

Reviews, 2014, 33: 224. https://doi.org/10.1016/j.rser.2014.02.002.

[3] Kim D-W., Yun U-J., Lee J-W et al. "Fabrication and operating characteristics of a flat tubular segmented-in-series solid oxide fuel cell unit bundle", Energy, 2014, 72: 215. https://doi.org/10.1016/j.energy.2014.05.026.

[4] Lee YD., Ahn KY., Morosuk T, Tsatsaronis G. "Environmental impact assessment of a solid-oxide fuel-cell-based combined-heat-and-power-generation system", Energy, 2015, 79: 455.

[5] Mazzucco A, Rokni M. "Thermo-economic analysis of a solid oxide fuel cell and steam injected gas turbine plant integrated with woodchips gasification", Energy, 2014, 76: 114. https://doi.org/10.1016/j.energy.2014.04.035.

[6] Mojaver P., Khalilarya S, Chitsaz A. "Multi-objective optimization using response surface methodology and exergy analysis of a novel integrated biomass gasification, solid oxide fuel cell and high-temperature sodium heat pipe system", Applied Thermal Engineering, 2019, 156: 627. https://doi.org/10.1016/j.applthermaleng.2019.04.104.

[7] Mounir H., Belaiche M., El Marjani A, El Gharad A. "Thermal stress and probability of survival investigation in a multi-bundle integrated-planar solid oxide fuel cells IP-SOFC (integrated-planar solid oxide fuel cell)", Energy, 2014, 66: 378. https://doi.org/10.1016/j.energy.2014.01.017.

[8] Yang B., Wang J., Zhang M et al. "A state-of-the-art survey of solid oxide fuel cell parameter identification: Modelling, methodology, and perspectives", Energy Conversion and Management, 2020, 213: 112856. https://doi.org/10.1016/j.enconman.2020.112856.

[9] Al-Sulaiman FA., Dincer I, Hamdullahpur F. "Exergy analysis of an integrated solid oxide fuel cell and organic Rankine cycle for cooling, heating and power production", Journal of Power Sources, 2010, 195: 2346. https://doi.org/10.1016/j.jpowsour.2009.10.075.

[10] Bao C., Shi Y., Croiset E et al. "A multi-level simulation platform of natural gas internal reforming solid oxide fuel cell–gas turbine hybrid generation system: Part I. Solid oxide fuel cell model library", Journal of Power Sources, 2010, 195: 4871. https://doi.org/10.1016/j.jpowsour.2010.01.078.

[11] Calise F., Dentice d'Accadia M., Palombo A, Vanoli L. "Simulation and exergy analysis of a hybrid Solid Oxide Fuel Cell (SOFC)–Gas Turbine System", Energy, 2006, 31: 3278. https://doi.org/10.1016/j.energy.2006.03.006.

[12] Chan SH., Ho HK, Tian Y. "Modelling of simple hybrid solid oxide fuel cell and gas turbine power plant", Journal of Power Sources, 2002, 109: 111. https://doi.org/10.1016/S0378-7753(02)00051-4.

[13] Chitgar N, Moghimi M. "Design and evaluation of a novel multi-generation system based on SOFC-GT for electricity, fresh water and hydrogen production", Energy, 2020, 197: 117162. https://doi.org/10.1016/j.energy.2020.117162.

[14] Gholamian E, Zare V. "A comparative thermodynamic investigation with environmental analysis of SOFC waste heat to power conversion employing Kalina and Organic Rankine Cycles", Energy Conversion and Management, 2016, 117: 150. https://doi.org/10.1016/j.enconman.2016.03.011.

[15] Ma S., Wang J., Yan Z et al. "Thermodynamic analysis of a new combined cooling, heat and power system driven by solid oxide fuel cell based on

ammonia–water mixture", Journal of Power Sources, 2011, 196: 8463. https://doi.org/10.1016/j.jpowsour.2011.06.008.

[16] Massardo AF, Lubelli F. "Internal Reforming Solid Oxide Fuel Cell-Gas Turbine Combined Cycles (IRSOFC-GT): Part A—Cell Model and Cycle Thermodynamic Analysis", Journal of Engineering for Gas Turbines and Power, 1999, 122: 27. 10.1115/1.483187.

[17] Ozcan H, Dincer I. "Thermodynamic Analysis of an Integrated SOFC, Solar ORC and Absorption Chiller for Tri-generation Applications", Fuel Cells, 2013, 13: 781. https://doi.org/10.1002/fuce.201300012.

[18] Peng MY-P., Chen C., Peng X, Marefati M. "Energy and exergy analysis of a new combined concentrating solar collector, solid oxide fuel cell, and steam turbine CCHP system", Sustainable Energy Technologies and Assessments, 2020, 39: 100713. https://doi.org/10.1016/j.seta.2020.100713.

[19] Tian M., Yu Z., Zhao H, Yin J. "Thermodynamic analysis of an integrated solid oxide fuel cell, Organic Rankine Cycle and absorption chiller trigeneration system with CO2 capture", Energy Conversion and Management, 2018, 171: 350. https://doi.org/10.1016/j.enconman.2018.05.108.

[20] Zabaniotou A. "Agro-residues implication in decentralized CHP production through a thermochemical conversion system with SOFC", Sustainable Energy Technologies and Assessments, 2014, 6: 34. https://doi.org/10.1016/j.seta.2014.01.004.

[21] Zhang S., Liu H., Liu M et al. "An efficient integration strategy for a SOFC-GT-SORC combined system with performance simulation and parametric optimization", Applied Thermal Engineering, 2017, 121: 314. https://doi.org/10.1016/j.applthermaleng.2017.04.066.

[22] Zhang X., Li J., Li G, Feng Z. "Cycle analysis of an integrated solid oxide fuel cell and recuperative gas turbine with an air reheating system", Journal of Power Sources, 2007, 164: 752. https://doi.org/10.1016/j.jpowsour.2006.11.031.

[23] Wang J., Yan Z., Ma S, Dai Y. "Thermodynamic analysis of an integrated power generation system driven by solid oxide fuel cell", International Journal of Hydrogen Energy, 2012, 37: 2535. https://doi.org/10.1016/j.ijhydene.2011.10.079.

[24] Yan Z., Zhao P., Wang J, Dai Y. "Thermodynamic analysis of an SOFC–GT–ORC integrated power system with liquefied natural gas as heat sink", International Journal of Hydrogen Energy, 2013, 38: 3352. https://doi.org/10.1016/j.ijhydene.2012.12.101.

[25] Zhao H., Jiang T, Hou H. "Performance analysis of the SOFC–CCHP system based on H2O/Li–Br absorption refrigeration cycle fueled by coke oven gas", Energy, 2015, 91: 983. https://doi.org/10.1016/j.energy.2015.08.087.

[26] Chitsaz A., Hosseinpour J, Assadi M. "Effect of recycling on the thermodynamic and thermoeconomic performances of SOFC based on trigeneration systems; A comparative study", Energy, 2017, 124: 613. https://doi.org/10.1016/j.energy.2017.02.019.

[27] Chitgar N., Emadi MA., Chitsaz A, Rosen MA. "Investigation of a novel multigeneration system driven by a SOFC for electricity and fresh water production", Energy Conversion and Management, 2019, 196: 296. https://doi.org/10.1016/j.enconman.2019.06.006.

[28] Emadi MA., Chitgar N., Oyewunmi OA, Markides CN. "Working-fluid selection and thermoeconomic optimisation of a combined cycle cogeneration dual-loop organic Rankine cycle (ORC) system for solid oxide fuel cell (SOFC) waste-heat recovery", Applied Energy, 2020, 261: 114384. https://doi.org/10.1016/j.apenergy.2019.114384.

[29] Adebayo V., Abid M., Adedeji M, Hussain Ratlamwala TA. "Energy, exergy and exergo-environmental impact assessment of a solid oxide fuel cell coupled with absorption chiller & cascaded closed loop ORC for multi-generation", International Journal of Hydrogen Energy, 2022, 47: 3248. https://doi.org/10.1016/j.ijhydene.2021.02.222.

[30] Zeng R., Guo B., Zhang X et al. "Study on thermodynamic performance of SOFC-CCHP system integrating ORC and double-effect ARC", Energy Conversion and Management, 2021, 242: 114326. https://doi.org/10.1016/j.enconman.2021.114326.

[31] Zhong L., Yao E., Zou H, Xi G. "Thermo-economic-environmental analysis of an innovative combined cooling and power system integrating Solid Oxide Fuel Cell, Supercritical CO2 cycle, and ejector refrigeration cycle", Sustainable Energy Technologies and Assessments, 2021, 47: 101517. https://doi.org/10.1016/j.seta.2021.101517.

[32] Dhahad HA., Ahmadi S., Dahari M et al. "Energy, exergy, and exergoeconomic evaluation of a novel CCP system based on a solid oxide fuel cell integrated with absorption and ejector refrigeration cycles", Thermal Science and Engineering Progress, 2021, 21: 100755. https://doi.org/10.1016/j.tsep.2020.100755.

[33] Mei S., Lu X., Zhu Y, Wang S. "Thermodynamic assessment of a system configuration strategy for a cogeneration system combining SOFC, thermoelectric generator, and absorption heat pump", Applied Energy, 2021, 302: 117573. https://doi.org/10.1016/j.apenergy.2021.117573.

[34] Song M., Zhuang Y., Zhang L et al. "Thermodynamic performance assessment of SOFC-RC-KC system for multiple waste heat recovery", Energy Conversion and Management, 2021, 245: 114579. https://doi.org/10.1016/j.enconman.2021.114579.

[35] Szargut J. Exergy Method: Technical and Ecological Applications. WIT Press; 2005.

[36] Saleh B. "Energy and exergy analysis of an integrated organic Rankine cycle-vapor compression refrigeration system", Applied Thermal Engineering, 2018, 141: 697. https://doi.org/10.1016/j.applthermaleng.2018.06.018.